ACS APPLIED MATERIALS & INTERFACES

Research Article

www.acsami.org

# Boosting Electrical Performance of High-$\kappa$ Nanomultilayer Dielectrics and Electronic Devices by Combining Solution Combustion Synthesis and UV Irradiation

Emanuel Carlos, Rita Branquinho,* Asal Kiazadeh, Jorge Martins, Pedro Barquinha, Rodrigo Martins, and Elvira Fortunato*

CENIMAT/i3N Departamento de Ciência dos Materiais, Faculdade de Ciências e Tecnologia (FCT), Universidade NOVA de Lisboa (UNL), and CEMOP/UNINOVA, 2829-516 Caparica, Portugal

Supporting Information

**ABSTRACT:** In the past decade, solution-based dielectric oxides have been widely studied in electronic applications enabling the use of low-cost processing technologies and device improvement. The most promising are the high-$\kappa$ dielectrics, like aluminum ($AlO_x$) and hafnium oxide ($HfO_x$), that allow an easier trap filling in the semiconductor and the use of low operation voltage. However, in the case of $HfO_x$, a high temperature usually is needed to induce a uniform and condensed film, which limits its applications in flexible electronics. This paper describes how to obtain $HfO_x$ dielectric thin films and the effect of their implementation in multilayer dielectrics (MLD) at low temperatures (150 °C) to apply in thin film transistors (TFTs) using the combination of solution combustion synthesis (SCS) and ultraviolet (UV) treatment. The single layers and multilayers did not show any trace of residual organics and exhibited a small surface roughness (<1.2 nm) and a high breakdown voltage (>2.7 MV $cm^{-1}$). The resulting TFTs presented a high performance at a low operation voltage (<3 V), with high saturation mobility (43.9 ± 1.1 $cm^2$ $V^{-1}$ $s^{-1}$), a small subthreshold slope (0.066 ± 0.010 V $dec^{-1}$), current ratio of 1 × $10^6$ and a good idle shelf life stability after 2 months. To our knowledge, the results achieved surpass the actual state-of-the-art. Finally, we demonstrated a low-voltage diode-connected inverter using MLD/IGZO TFTs working with a maximum gain of 1 at 2 V.

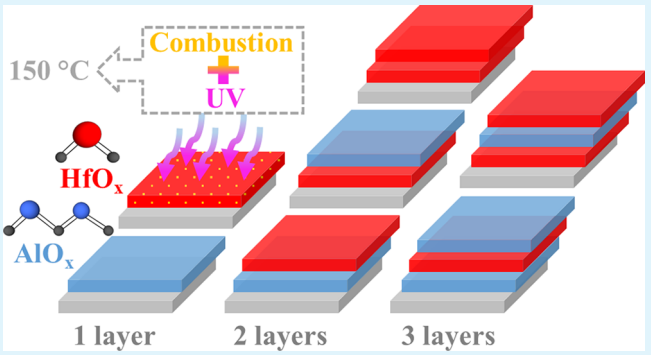


**KEYWORDS:** *low temperature, nanomultilayer dielectric oxides ($AlO_x$ and $HfO_x$), DUV irradiation, solution combustion synthesis, low operating voltage TFTs*

## 1. INTRODUCTION

Technology has been growing exponentially, leading to the necessity of low-cost processes and materials that allow a more sustainable world. For that, printable, flexible, disposable, and transparent electronics have been highly explored.[1,2] However, the typical fabrication techniques for oxide films and devices are vacuum-based techniques, like atomic layer deposition and chemical and physical vapor deposition. These techniques require expensive high-vacuum equipment, resulting in high production costs.[1] For the production of printed electronics, suitable materials and optimized processes or techniques with low-cost manufacturing need to be identified and developed. As a result, solution-based thin films have gained a lot of attention due to the low cost, simplicity and good film uniformity in large areas.[3] Spin-coating, screen printing, inkjet printing, bar-coating, and spray pyrolysis are the most-used techniques for solution processing oxide semiconductors and gate dielectrics.[3−7] Actually, choice of suitable functional/active materials that can be printed is essential for the performance of the printed electronic devices. In thin film transistors, the semiconductor layer has been used in organics and inorganics (oxides) with high success at low temperature.[8,9]

The insulator layer plays a crucial role in the devices performance too, by mainly defining the devices stability and operation voltages.[8−11] Also, the solution process of this layer has been frequently used, either for organics or oxides materials. In the case of organic materials, PVA or PVP are possible alternatives;[12−14] however, these have some setbacks, such as the operation voltage control with the decrease in thickness, low carrier mobility, and instability issues, which limit their application.[8,9,11] By using solution-based high-$\kappa$ inorganic dielectrics is possible to enhance the capacitance coupling between the gate dielectric and the channel layer in TFTs. As a result, the subthreshold slope is improved and the operating voltage is reduced leading to low consumption electronic devices.[15,16] Moreover, the use of multilayers allows the

Received: August 7, 2017
Accepted: November 1, 2017
Published: November 1, 2017





DOI: 10.1021/acsami.7b11752
ACS Appl. Mater. Interfaces XXXX, XXX, XXX−XXX

Table 1. Literature of Developed High-$\kappa$ Solution-Based Hafnium Oxide Single Layers and Multilayers Applied in TFTs

| Year | TFT (dielectric/semiconductor) | $T$ (°C) | SS (V dec$^{-1}$) | $\mu_{SAT}$ (cm$^2$ V$^{-1}$ s$^{-1}$) | $I_{ON/OFF}$ | $V_{ON}$ (V) | $V_G$ range (V) |
|---|---|---|---|---|---|---|---|
| 2012[17] | ($HfO_x$ \|$AlO_x$)/ ZTO | 400 | 0.12 | 3.8 | $1 \times 10^5$ | 0.4 | −2 to 3 |
| | ($AlO_x$ \|$HfO_x$)/ ZTO | | 0.16 | 1.2 | | −0.2 | |
| 2012[25] | ($HfO_x$)/ZTO | 300 | 0.11 | 1.1 | $1 \times 10^7$ | 0.2 | −5 to 5 |
| 2015[26] | ($HfO_x$)/HIZO | 500 | 1.1 | 3.6 | $1 \times 10^4$ | −0.1 | - 5−10 |
| 2015[27] | ($HfO_x$)/ZnO | 380 | | 42 ± 1.4 | $1 \times 10^7$ | −0.4 | −1 to 6 |
| 2015[16] | ($HfO_x$)/IZO | 300 | 0.72 | 25.7 | $1 \times 10^6$ | 1.5 | −1 to 5 |
| | | 200 | 1.32 | 6.2 | $1 \times 10^3$ | 0.8 | |
| 2017[15] | ($HfO_x$)/ZTO | 350 | 0.07 | 13.2 | $1 \times 10^8$ | −0.1 | −1−2 |
| present study | ($HfO_x$)/IGZO | 150 | 0.082 ± 0.002 | 31.2 ± 1.4 | $1 \times 10^5$ | −0.04 ± 0.05 | −1−2 |
| | ($HfO_x$ \|$HfO_x$)/ IGZO | | 0.066 ± 0.010 | 43.9 ± 1.1 | $1 \times 10^6$ | 0 ± 0.03 | −1−2 |
| | ($HfO_x$ \|$AlO_x$)/ IGZO | | 0.076 ± 0.009 | 23.6 ± 0.6 | $1 \times 10^5$ | 0.01 ± 0.03 | −1−2 |
| | ($HfO_x$\|$AlO_x$\|$HfO_x$)/IGZO | | 0.101 ± 0.004 | 37.5 ± 2.2 | | 0.03 ± 0.06 | −1−3 |
| | ($AlO_x$ \|$HfO_x$)/IGZO | | 0.099 ± 0.019 | 37.2 ± 1.9 | | −0.01 ± 0.06 | −1−2 |
| | ($AlO_x$\|$HfO_x$\|$AlO_x$)/IGZO | | 0.133 ± 0.013 | 30.5 ± 1.8 | | −0.09 ± 0.09 | −1−3 |

insulator to achieve remarkable properties with just one material (e.g., high-$\kappa$ and band gap).[17,18] The most used inorganic dielectrics are zirconium oxide ($ZrO_2$), tantalum oxide ($Ta_2O_5$), aluminum oxide ($Al_2O_3$), hafnium oxide ($HfO_2$) and their mixtures.[3,17,19−21] The larger capacitance obtained with these allows a higher density of charges induced in the semiconductor, which lead to an easier trap filling. Solution-processed $Al_2O_3$ and $HfO_2$ are the most promising candidates, with high dielectric constant, 9 and 25 respectively, and in the case of $HfO_2$ a lower bandgap (5.8 eV) when compared with $Al_2O_3$ (8.9 eV).[11,15] Because the bandgap is smaller in the case of $HfO_2$, the carrier injection is easier than in $Al_2O_3$.[17,22] However, these materials needed high annealing temperatures, so new methods and techniques have been developed, like solution combustion synthesis (SCS) and deep ultraviolet (DUV) treatment, to obtain high-quality films at low temperature that are compatible with low-cost flexible substrates.[8,9] In the case of SCS, an oxidizer (nitrates) and a fuel (urea, citric acid) are added to the precursor solution. During the annealing process a exothermic reaction occurs, resulting in a reduction of the external heat required for the film formation; the remove of organic solvents and film densification.[9,19] By using a DUV treatment, the films are exposed to high-energy photons, which causes the cleavage of alkoxy groups, active metals, and oxygen atoms to simplify M−O−M network formation. After less than 10 min of UV irradiation, the polymeric chains break into smaller fragments, which induces degradation, leading to removal of oxygen, carbon and improving the film densification.[11,23,24] The combination of these methods improves the reliability of the nanoscale film morphology, composition of metal oxides and stability over time. The additional energy provided by the exothermic combustion reaction contributes to enhanced film densification in a short annealing time.

In this work, we report for the first time the combination between the solution combustion synthesis (SCS) and deep ultraviolet (DUV) treatment in $HfO_x$ single and nanomultilayer dielectrics (composed by $AlO_x$ and $HfO_x$ thin films) at low temperature (150 °C) in gallium-indium-zinc oxide (IGZO) TFTs (Table 1). The effects of increasing the number of dielectric layers in the electric performance were investigated using different characterization techniques. Finally, stable and low voltage ($HfO_x$|$HfO_x$)/IGZO TFTs have been applied to a diode-connected inverter.

## 2. EXPERIMENTAL DETAILS

**2.1. Precursor Solution Preparation and Characterization.** Aluminum nitrate nonahydrate ($Al(NO_3)_3{\cdot}9H_2O$, Fluka, 98%) was dissolved in 2-methoxyethanol (2-ME, $C_3H_8O_2$, ACROS Organics, 99%), to yield solution with an $Al^{3+}$ ion concentration of 0.1 M. Urea ($CO(NH_2)_2$, Sigma, 98%) was then added to the prepared solution which was maintained under constant stirring for at least 1 h. The urea to aluminum nitrate molar proportion was 2.5:1, to guarantee the redox stoichiometry of the reaction.[19] Hafnium chloride-based precursor ($HfCl_4$, Alfa Aesar, 99.9%) was dissolved in 2-methoxyethanol (2-ME, $C_3H_8O_2$, ACROS Organics, 99%) and maintained under constant stirring for 4 h. Then the oxidizing agent, ammonium nitrate ($NH_4NO_3$, Roth, 98%) and the fuel, urea was added and stirred at least 2 h for a concentration of 0.1 M. For the ammonium nitrate precursor, the urea molar proportion was 1:(1/3). All precursor solutions were filtrated through 0.20 $\mu$m hydrophilic filters before use.

The precursor's solvent evaporation with a rotatory evaporator (Heidolph, model Hei-VAP Value/G3) was done before the thermogravimetry and differential scanning calorimetry (TG-DSC) at 70 °C with a rotation of 50 rpm during 1 h 30 min. A thermal characterization of precursors was then performed by TG-DSC under air atmosphere up to 500 °C with a 10 °C min$^{-1}$ heating rate in an aluminum crucible using a simultaneous thermal analyzer, Netzsch (TG-DSC - STA 449 F3 Jupiter). The optical properties were obtained using a PerkinElmer lambda 950 UV/vis/NIR spectrophotometer by measuring absorbance (A) in the wavelength range of 190−400 nm.

**2.2. Dielectric Deposition and Characterization.** Prior to deposition all substrates (silicon wafer and corning glass with an area of 2.5 × 2.5 cm$^2$) were cleaned in an ultrasonic bath at 60 °C in acetone for 10 min, then in 2-isopropanol for 10 min and dried under nitrogen ($N_2$); followed by a 10 min UV/Ozone surface activation step in a PSD-UV Novascan system. Thin films were deposited by spin coating, forming a single layer ($AlO_x$; $HfO_x$) and multilayers ($AlO_x$|$HfO_x$; $AlO_x$|$HfO_x$|$AlO_x$; $HfO_x$|$HfO_x$; $HfO_x$|$AlO_x$; $HfO_x$|$AlO_x$|$HfO_x$) using the $AlO_x$ and $HfO_x$ precursor solutions with a concentration of 0.1 M for 35 s at 2000 rpm (Laurell Technologies). That was followed by an immediate thermo annealing at 150 °C assisted by ultraviolet irradiation (UV) (PSD Pro Heated Series, PSDP-UVT Novascan system; emission wavelengths of 253.7 (90%) and 184.9 nm (10%); area of 20 × 20 cm$^2$) at a lamp distance of 2 cm (the output energy intensity of the lamp was 75 mW·cm$^{-2}$ at 254 nm) for 30 min each layer in nitrogen ambient, with a gas flow of 240 mbar. The films structure was assessed by glancing angle X-ray diffraction (GAXRD) performed by an X'Pert PRO PANalytical powder diffractometer using Cu K$\alpha$ line radiation ($\lambda$ = 1.540598 Å) with an angle of incidence of the X-ray beam fixed at 0.9°. The surface morphology was investigated by atomic force microscopy (AFM, Asylum MFP3D) and the film thickness by scanning electron microscopy analysis of a sample cross-section prepared by focused ion beam using $Ga^+$ ions (SEM-FIB, Zeiss


DOI: 10.1021/acsami.7b11752
ACS Appl. Mater. Interfaces XXXX, XXX, XXX−XXX

Auriga Crossbeam microscope). Fourier Transform Infra-Red (FTIR) spectroscopy characterization of thin films deposited on Si substrates were recorded using an attenuated total reflectance (ATR) sampling accessory (Smart iTR) equipped with a single bounce diamond crystal on a Thermo Nicolet 6700 Spectrometer. The spectra were acquired with a 45° incident angle in the range of 4500−540 $cm^{-1}$ and with a 4 $cm^{-1}$ resolution.

**2.3. Electronic Device Fabrication and Characterization.** Metal−insulator−semiconductor (MIS) capacitors were produced by depositing a single layer, $AlO_x$ or $HfO_x$, and multilayers onto p-type silicon substrates (1−10 Ω·cm) as described above. Aluminum electrodes (80 nm thick) with an area of $1.96 \times 10^{-3}$ $cm^2$ were deposited by thermal evaporation via shadow mask on top of the insulators, with similar but unpatterned electrodes being also deposited on the back of the silicon wafer. Electrical characterization was performed measuring both the capacitance−voltage and capacitance-frequency characteristics in the range of 1 kHz to 1 MHz of frequency using a semiconductor parameter analyzer (Keithley 4200SCS) and probe station (Janis ST-500). The TFTs were produced in a staggered bottom-gate, top-contact structure by depositing the single layers or the nanomultilayers onto p-type silicon substrates acting as gate electrodes.

The IGZO semiconductor film (30 nm thick) was sputtered onto the dielectric thin films via shadow mask for all temperatures. The deposition was performed using a commercial IGZO ceramic target (2:1:2 In:Ga:Zn atomic ratio) by rf magnetron sputtering in an Ar+$O_2$ atmosphere without intentional substrate heating in an AJA 1300-F system.[28]

Finally, source and drain aluminum electrodes (80 nm thick) were deposited by thermal evaporation via shadow mask onto the films. Hereafter the IGZO TFTs were annealed at 150 °C, for 1 h in air. An 80 nm thick aluminum film was also deposited on the back of the silicon wafer.

The current−voltage characteristics of the devices were obtained in double sweep mode in ambient conditions using a semiconductor parameter analyzer (Agilent 4155C) attached to a microprobe station (Cascade M150) inside a dark box, at room temperature.

The saturation mobility ($\mu_{SAT}$) was determined from the following equation

$$I_D = \left(\frac{C_{ox} W \mu_{SAT}}{2L}\right)(V_G - V_T)^2 \quad (1)$$

where $C_{ox}$ is the gate dielectric capacitance per unit area, the channel length ($L$) and width ($W$) are 90 and 1000 μm, $V_G$ is the gate voltage, and $V_T$ is the threshold voltage, which was determined in the saturation region by linear fitting of a $I_D^{1/2}$ vs $V_G$ plot.

Gate bias stress tests were performed on TFTs with one and two layers of dielectric under air environment by applying a constant gate voltage (0.5 MV $cm^{-1}$ electric field) for 1 h, after which the devices were allowed to recover. Transfer characteristics were measured at fixed time intervals during stress and recovery processes.

To investigate the possibility of solution-based TFTs in circuit application, we constructed the inverter structure with two TFTs in different substrates. A semiconductor parameter analyzer (Keysight B1500A) was used for the DC characterization of the inverter. For transient measurements of the inverter, the input waveforms were generated by a function generator (Wavetek 395) and the output signal was acquired by an oscilloscope (ISO-TECH IDS 8062).

## 3. RESULTS AND DISCUSSION

Solution combustion synthesis of nanomaterials has been crucial for the fabrication of high-quality metal oxides at low temperature.[9] In combustion synthesis at certain temperature, a violent redox reaction between an organic fuel, urea, and the oxidizer, ammonium nitrate, occurs, related with the release of massive reaction heat. This local heat results in the increase of local temperature inside the dielectric films, which promotes the precursors conversion into oxides at low temperature.[19]

Since 2011, the solution combustion synthesis of $AlO_x$ thin films applied in TFTs has been reported; however, for $HfO_x$, only a few results have succeeded with high-performance TFTs requiring high temperatures (Table 1).[9,15,29]

The solution combustion synthesis of $HfO_2$ from hafnium chloride and ammonium nitrate (oxidizer), and urea (reducing agent) can be represented by the combination of ammonium nitrate decomposition reaction (eq 2) and urea oxidation reaction (eq 3).

$$HfCl_4 + 4NH_4NO_3 \rightarrow HfO_2 + 6H_2O + 4N_2 + 4HCl \quad (2)$$

$$CO(NH_2)_2 + \left(\frac{3}{2}\right)O_2 \rightarrow 2H_2O + CO_2 + N_2 \quad (3)$$

The overall reaction can thus be written as bellow (eq 4):

$$3HfCl_4 + 12NH_4NO_3 + 4CO(NH_2)_2 \rightarrow 3HfO_2 + 16N_2 + 4CO_2 + 26H_2O + 12HCl \quad (4)$$

This is a theoretical reaction equation that neglects possible secondary reactions, although, it allows the calculation of a stoichiometric condition that can be used as a reference.[30] In the oxide formation, the chemistry of the redox reaction is determinant for the thermodynamics, particularly, the nature of the reagents and the fuel/oxidizer ($\phi$).[30]

The optimal stoichiometry composition of the redox mixture is obtained for $\phi = 1$; however, to achieve lower temperatures in the thin film formation, as shown by DSC-TG analysis (Figure 1 a), was used $\phi = 1.1$. In this composition, the redox mixture is under fuel-rich condition, requiring molecular oxygen to fully convert the fuel.[31,32] The oxidizing/reducing characteristics of a mixture can be calculated by the Jain method, which is based on propellant chemistry.[33] In this

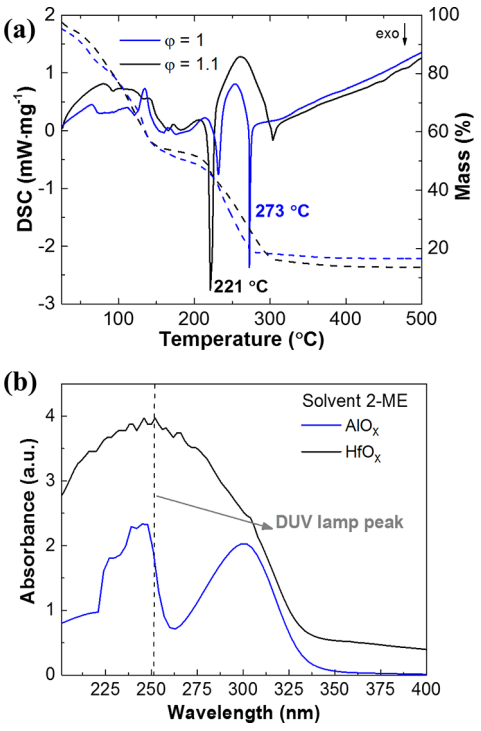


**Figure 1.** (a) TG-DSC analysis of $HfO_x$ precursor solution and (b) absorbance spectra of both $AlO_x$ and $HfO_x$ precursor solutions.



DOI: 10.1021/acsami.7b11752
ACS Appl. Mater. Interfaces XXXX, XXX, XXX−XXX

method carbon and hydrogen are considered as reducing elements with final valences of +4 and +1, respectively; hafnium metal ions are also considered reducing elements with a final valence of +4. Oxygen and nitrogen are considered oxidizers with their final valences of −2 and 0, respectively. The reducing valence of urea is +6 and the oxidizing valence of ammonium nitrate is −2 as calculated by the Jain method hence (1/3) mol of urea are required per mole of the nitrate precursor (ammonium nitrate) to ensure redox stoichiometry. In this condition, to minimize the generation of cracks and pores in metal oxide films, which can significantly contribute to leakage current in the vertical direction, deep ultraviolet (DUV) treatment was used.[8,10] The condensation and film densification in metal oxides are improved with DUV irradiation in nitrogen environment; however, some ozone ($O_3$) is also formed, which in this case helps to fully convert the fuel in the combustion reaction at low temperatures.

**3.1. Precursor Solution Characterization.** Thermal analysis of precursor solutions was performed to investigate the decomposition behavior of the hafnium oxide precursors with different stoichiometry compositions. Figure 1a shows the differential scanning calorimetry (DSC) and thermogravimetry (TG) of the $HfO_x$ up to 350 °C, as above this temperature no further events were observed. The most promising precursor solution with a fuel rich condition, $\phi$ = 1.1, exhibits an intense exothermic peak at 221 °C and small peak at 304 °C, which is attributed to the combustion reaction of residual fuel resulting in a mass loss of 40%. Also, two endothermic peaks were observed at 139 and 172 °C, which are related to the solvent evaporation and some residual organics. In the case of the stoichiometry condition, $\phi$ = 1, the precursor solution show a smaller exothermic peak at 232 °C and the most intense one at 273 °C, which is higher than the fuel rich condition. Thermal analysis indicates that the minimum temperature required for full degradation is 304 °C. The DSC-TG analysis 2-ME based of $AlO_x$ precursor solutions, has been previously reported by our group,[34] and shows an intense exothermic peak at 176 °C corresponding to oxide formation, and a residual endothermic peak at 250 °C attributed to the degradation of residual organics. The difference in combustion reaction temperature of $HfO_x$ and $AlO_x$ is expected as it depends on the specific bonding energy of the ligands with the metal ions in solution which varies from metal to metal, as reported by Epifani et al.[35]

The absorbance of the precursor solutions in the UV−vis range was performed to assess the efficiency of irradiation with a DUV lamp with a maximum emission at 254 nm (90%) to enhance film condensation and densification.[8,24] Figure 1v shows that both solutions absorb in that wavelength, being more significant for the hafnium oxide precursor solution. Therefore, DUV treatment is expected to contribute to degradation of organic residuals and decreasing the temperature required for the formation of M-O-M.[8]

**3.2. Dielectric Thin Film Characterization.** The optical transmission of single and multilayer thin films was measured. Figure 2 shows that all films are highly transparent (>89%) in the visible range. However, with an increase in the number of layers and film thickness, total transmittance is slightly decreased. The optical bandgap ($E_g$), determined via Tauc plot analysis is 4.9 eV for $HfO_x$ thin films, as shown in Figure 2. This value is lower than the expected 5.8 eV reported for physical vapor deposition (PVD) techniques.[15,22] $HfO_x$ thin films produced by solution may have some residual chloride species which slow down the dehydroxylation process and

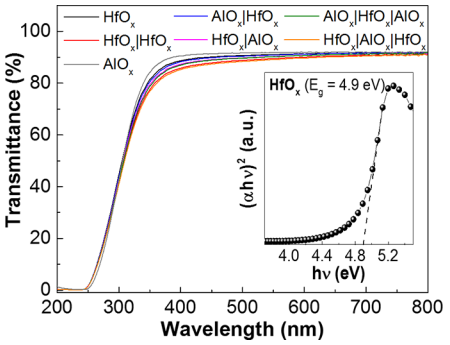


**Figure 2.** Optical transmittances of the single and multilayer dielectric thin films. The inset shows the Tauc plot of $HfO_x$.

increase the amount of oxygen vacancies in the thin film, which results in a decrease of the bandgap energy due to the increasing of density of states.[15] The bandgap of the other layers was not obtained because of the presence of aluminum oxide, which has a large bandgap (8.9 eV) unable to be measured using Tauc plot analysis.[36]

The dielectric thin films produced were characterized with ATR-FTIR before and after annealing, as shown in Figure 3a. All samples show an absorbance peak at 1107 $cm^{-1}$ attributed to the Si−O transversal optic stretching.

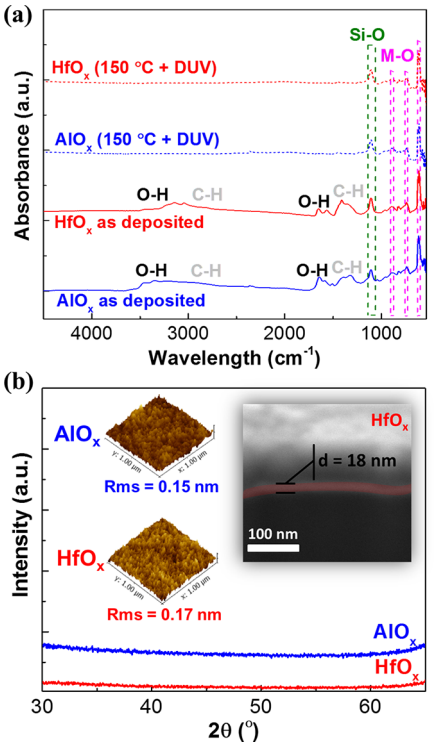


**Figure 3.** (a) FTIR spectra of $AlO_x$ and $HfO_x$ thin films before and after annealing; (b) XRD diffractograms, AFM deflection images (1 × 1 $\mu m^2$) of both dielectric thin films, and high-resolution SEM-FIB cross-section image of $HfO_x$ thin film.

Prior to annealing absorption bands related to organic precursors in the film can be observed, namely, a broad band between 3700 and 3000 $cm^{-1}$ and bands at 1630 and 1575 $cm^{-1}$ assigned to O−H stretching vibrations associated with water absorption and OH increase; weak absorption bands between 3090 and 2800 $cm^{-1}$ associated with the C−H stretch


DOI: 10.1021/acsami.7b11752
ACS Appl. Mater. Interfaces XXXX, XXX, XXX−XXX

and between 1500 and 1300 $cm^{-1}$ with C−H deformation and carbonate.[37] After annealing at 150 °C assisted by DUV treatment, none of these bands were observed, confirming the elimination of all residual organics.

The absorption peaks at 889, 739−748, and 611−601 $cm^{-1}$ are attributed to the presence of metal oxide (M−O) chemical bonds, Hf−O and Al−O.[37−39] The FTIR analysis of multilayer thin films showed similar results, as depicted in Figure S1.

The structure of the solution based dielectric thin films was investigated by X-ray diffraction (XRD). The absence of diffraction peaks in Figure 3b reveals that amorphous thin films are obtained in the single layer and multilayer samples (see Figure S2). Amorphous materials have less grain boundaries and are expected to have a small surface roughness, low leakage current, and high breakdown voltage.[29]

Atomic force microscopy (AFM) images were used to analyze the surface morphology. The lowest roughness was observed for single layers, $AlO_x$ and $HfO_x$, 0.15 and 0.17 nm, respectively, as depicted in Figure 3b. Figure S3 shows that all multilayer samples have a smooth surface morphology and a surface roughness bellow 1.2 nm. The surface morphology was not affected by the release of dichloride during the combustion reaction.[15] The low surface roughness leads to a better interface between the dielectric layer and the IGZO improving the electrical performance.

High-resolution SEM-FIB cross-section imaging of all the dielectric multilayer thin films was performed to measure the films thickness. Single layer $HfO_x$ thin film has a thickness of about 18 nm (Figure 3b); multilayer films have a thickness of about 26 nm for $HfO_x|HfO_x$, 28 nm for $HfO_x|AlO_x$, 44 nm for $HfO_x|AlO_x|HfO_x$, 30 nm for $AlO_x|HfO_x$, and 44 nm for $AlO_x|HfO_x|AlO_x$ (see Figure 4 and Figure S4). To demonstrate a better film densification achieved with the combination of UV treatment and combustion synthesis, a study was done with $AlO_x$ for different concentrations showing thinner films when combustion method with UV was used (see Figure S5). The film densification is more significant for higher concentration because of the higher amount organics to be decomposed; nevertheless, the film degradation is relevant regardless of the film densification.

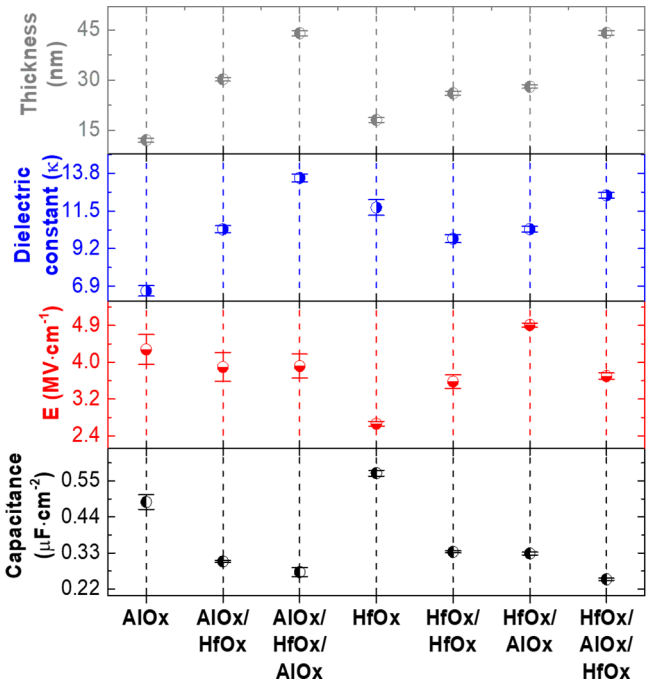


**Figure 4.** Statistical analysis of capacitance measured at 1 kHz, dielectric thickness, breakdown voltage, and dielectric constant of all dielectric thin films.

**3.3. Dielectric Multilayer Electrical Characterization.** The increasing number of high-$\kappa$ dielectric layers using combustion synthesis and DUV treatment were studied to determine the best dielectric composition and dielectric/semiconductor interface. The electrical characterization of all dielectrics was performed by measuring the capacitance−voltage ($C-V$), capacitance-frequency ($C-f$), and breakdown voltage ($E$) of metal−insulator-semiconductor (MIS) structures, see Figure S6.

In order to clarify the dielectrics performance a statistical analysis was done, as depicted in Figure 4 and Table S1. Higher dielectric constants for the multilayer dielectrics with three layers, $AlO_x|HfO_x|AlO_x$ (13.5) and $HfO_x|AlO_x|HfO_x$ (12.5) were obtained, as depicted in Figure 4. However, dielectric constant is slightly higher for the $AlO_x|HfO_x|AlO_x$ due to the higher capacitance of the multilayer. In the case of $HfO_x$, the highest dielectric constant was obtained, as expected, but when you add a second layer of $HfO_x$, the dielectric constant decreases because the thin film produced has more residual chloride species. This species will slow down the dehydroxylation process and increase the amount of oxygen vacancies in the thin film, which affects the dielectric constant.[15] In the other cases, when a layer of $HfO_x$ in $AlO_x$ is added, the dielectric constant increases because of the higher dielectric constant of $HfO_x$. The breakdown voltage using a single layer of $HfO_x$ was improved from 2.7 MV $cm^{-1}$ to 3.6 MV $cm^{-1}$ with a bilayer due to the thickness increase and interface quality. The highest breakdown field of 4.9 MV $cm^{-1}$ was achieved for the $HfO_x|AlO_x$ multilayer, which was also enhanced when compared with the $AlO_x|HfO_x$ multilayer, 4.3 MV·$cm^{-1}$, meaning a better interface when $AlO_x$ is in the top of $HfO_x$, as shown in Figure 4. $HfO_x$ presents a lower band gap facilitating carrier injection when compared to $AlO_x$. Also, the fact that $HfO_x$ precursor contains chlorides leads to increased interface charge defects. Therefore, a higher breakdown voltage is achieved when the $AlO_x$ is deposited over HfOx. To further improve the $AlO_x|HfO_x$ interface quality, a longer annealing could be performed.

By increasing the number of layers, the capacitance decrease showing fairly a constant value over the range of frequencies, as presented in Figure S6a.

Hysteresis starts to increase in the capacitance−voltage characteristics of the MIS structure, with the increase of the number of layers, as shown in Figure S6b. The flat band voltage is changed with respect to the different layer composition and increasing the number of layers. The $HfO_x$ bilayer shows less hysteresis change when compared with a single layer of $HfO_x$.

Taking into account the properties achieved, the most promising dielectrics were all the ones with more than one layer.

**3.4. Low Voltage Multilayer TFTs.** All the TFTs produced at low temperature (150 °C) demonstrated low voltage operation (maximum 3 V) and exhibited a good electrical performance with low gate leakage current. To our knowledge this is the first time that TFTs with a single layer of $HfO_x$ and multilayers combining $AlO_x$ and $HfO_x$ solution based dielectrics are reported at 150 °C. This was possible by the


DOI: 10.1021/acsami.7b11752
ACS Appl. Mater. Interfaces XXXX, XXX, XXX−XXX

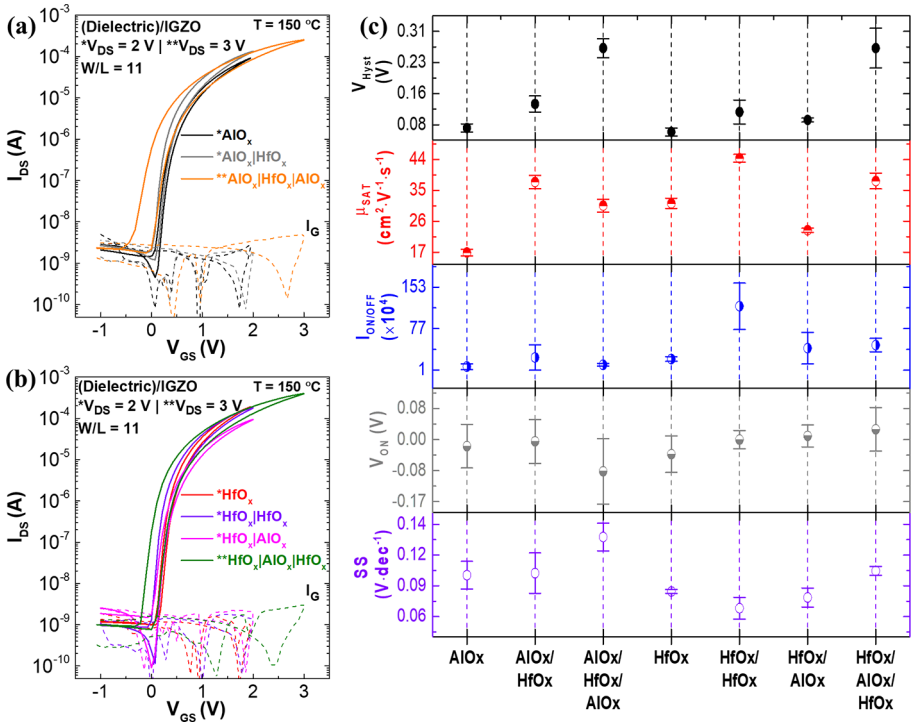


**Figure 5.** (a, b) Typical transfer characteristics of the single and multilayers insulator thin films applied in IGZO TFTs; (c) statistical distributions of device parameters, hysteresis ($V_{Hyst}$), saturation mobility ($\mu_{SAT}$), current on−off ratio ($I_{ON/OFF}$), turn-on voltage ($V_{ON}$) and subthreshold slope (SS).

combination of thermal annealing with deep-ultraviolet (DUV) irradiation to enhance the intrinsic properties of the films, resulting in more uniform and compact films and by using a slightly fuel-rich solution combustion synthesis (SCS) which decreased the ignition temperature of the exothermic reaction, and hence the M-O-M formation. Typical transfer curves of the TFTs can be observed in Figure 5a, b and the output curves in Figure S7. Figure 5b shows that using $HfO_x$ layer instead of $AlO_x$ in contact with the gate electrode facilitates carrier injection because of the lower bandgap, resulting in an improved interface and lower off current.

To study the uniformity and reproducibility of these devices a set of 15 devices was produced and characterized for all the dielectric thin films, as shown in Figure 5c. This analysis was assessed through the measurement of the turn-on voltage ($V_{ON}$), hysteresis ($V_{Hyst}$), drain current on−off ratio ($I_{ON}/I_{OFF}$), subthreshold slope (SS), and saturation mobility ($\mu_{SAT}$), which was calculated using the dielectric capacitance measured in MIS devices at a frequency of 1 kHz (see Table S1). High mobility that surpassed the state-of-the-art was obtained for all the multilayer dielectric TFTs. The highest mobility, 43.9 ± 1.1 $cm^2\ V^{-1}\ s^{-1}$, was achieved for the bilayer of $HfO_x|HfO_x$-based TFTs. The roughness at the $HfO_x|AlO_x$ surface may form interface charge traps, which increase the carrier scattering centers, explaining the lower mobility obtained.[16] Other reasons for the high carrier mobility achieved for the solution-based dielectrics IGZO TFTs are the indium content in the IGZO semiconductor and the high areal capacitance of the dielectrics used.[16] In terms of on/off current ratio, most of the devices show $1 \times 0^5$. We note that a ratio of $1 \times 10^6$ is achieved for devices with a bilayer of $HfO_x$, which is high when compared with literature (Table 1). The turn-on voltage of most devices was close to 0. The $HfO_x|HfO_x$ multilayer exhibited less variation of turn-on voltage in different devices. The lowest subthreshold slope (SS) value of 0.066 ± 0.01 V $dec^{-1}$ was obtained for $(HfO_x|HfO_x)$/IGZO TFTs, indicating the enhanced quality of dielectric-semiconductor interface.

All devices showed an anticlockwise hysteresis, as shown in Figure 6a, because of mobile ions, namely some organic residues or defects in the gate dielectric. This is a consequence of using a low temperature (150 °C), which can be surpassed by performing a longer annealing time with DUV treatment or using higher temperature.

To determine how device performance is affected after aging in air environment, TFTs were again characterized after 2 months. The IGZO TFT with the solution-based $AlO_x|HfO_x$ dielectric showed a slight SS degradation, whereas, the SS of $AlO_x|HfO_x|AlO_x$ multilayer device was larger, as shown in Figure S8 and Table S2. The impact of humidity on the degraded on/off ratio of aged-devices based on the $HfO_x|AlO_x|HfO_x$ multilayer was also observed .[11] To improve the quality in the interfaces of layers, longer annealing should be performed and in addition, a device passivation is also suggested.[28] All other devices with one and two dielectrics layers showed good stability over time, with only a slight variation of the electrical parameters. The $(HfO_x|HfO_x)$/IGZO TFTs revealed the best switching behavior over time, from 0.061 to 0.068 V $dec^{-1}$, as depicted in Figure 6a.

To investigate the devices operational stability, we performed a positive and negative gate bias stress in air environment by applying a constant gate voltage equivalent to electrical field of ±0.5 MV $cm^{-1}$ while keeping the source and drain electrodes grounded. The multilayer devices with 3 layers were not examined due to their instability over time, and also the $AlO_x$ single layer did not show an improved performance when compared with literature.[11,24] The other devices were stressed for 1 h, combined with ∼2 h recovery time in dark condition. Transfer characteristics were obtained in the saturation regime ($V_{DS}$ = 2 V) at selected times during stress and recovery processes, as shown in Figure S9 and S10. Figure 6b shows the


DOI: 10.1021/acsami.7b11752
ACS Appl. Mater. Interfaces XXXX, XXX, XXX−XXX

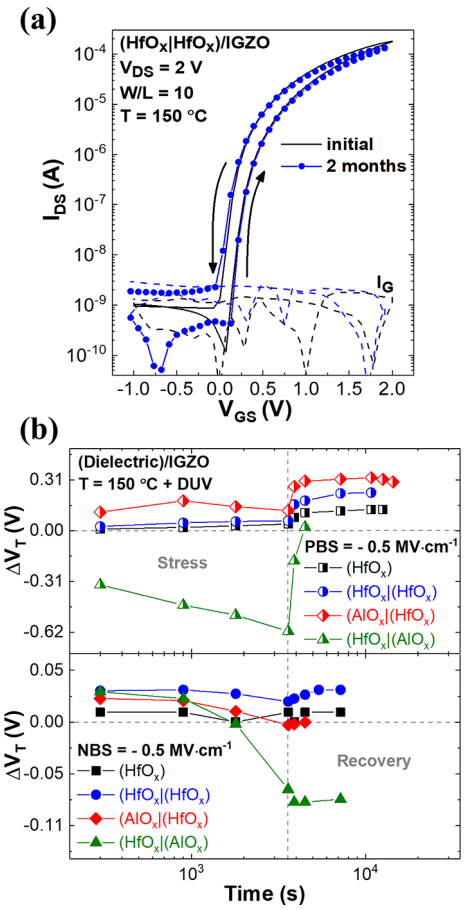


**Figure 6.** (a) Aging effect of $(HfO_x|HfO_x)$/IGZO TFTs after 2 months; (b) threshold voltage variation ($\Delta V_T$) during a 0.5 MV cm$^{-1}$ stress in selected dielectrics under PBS and NBS tests for 1 h in air environment.

threshold voltage variation ($\Delta V_T$) with time during stress and recovery phases.

By applying a positive gate bias stress (PBS) a maximum $V_T$ shift of -0.61 V is obtained for the $HfO_x|AlO_x$ multilayer based TFTs. The negative threshold voltage shift under positive gate bias stress of a device employing the $AlO_x$ gate dielectric has been reported in a previous publication, where this phenomenon was related to the release of hydrogen from the dielectric to the semiconductor.[7]

The TFTs with $AlO_x|HfO_x$ multilayer, having the $HfO_x$ in contact to the channel show dual shift of threshold voltage (see Figure S8). Simultaneously, two mechanisms contribute for the TFT instability: (i) Negative shift related to the $AlO_x$ layer[7] and (ii) charge trapping into the dielectric and/or at the interface of channel and dielectric (HfOx) which results in the positive shift of threshold voltage. Interestingly, the electron donating effect happens although the $AlO_x$ layer is not located at the interface to the semiconductor. This means that the hydrogen can easily penetrate into the $HfO_x$ layer.

The TFTs with $HfO_x|AlO_x$ in contact to the channel are recovered in 15 min, whereas the ones with $AlO_x|HfO_x$ are not fully recovered after 3 h of rest in dark condition. The single and bilayers of $HfO_x$ applied in IGZO TFTs were the ones that presented lower positive $V_T$ shift under PBS. However, after removing the stress, the threshold voltage is still shifting toward the positive direction even more pronounced than when the TFT is under PBS (see Figure S9). The recovery of the devices to the initial state can be only achieved by a reannealing process of the TFTs. It is possible that this shows how under PBS compensating acceptor defects are created which persist beyond the stressing. In addition, the residual Cl may be a strong candidate for an extra trap sites in the HfOx layer.[15] Further investigations are required to elucidate the mechanism at the $HfO_x$/IGZO interface, which leads to the absence of recovery.

The $V_T$ under negative gate bias stress (NBS) for the different conditions showed a small negative shift with negligible degradation of SS, which is frequently reported for n-type semiconductor TFTs (see more detail Figure S10).[40]

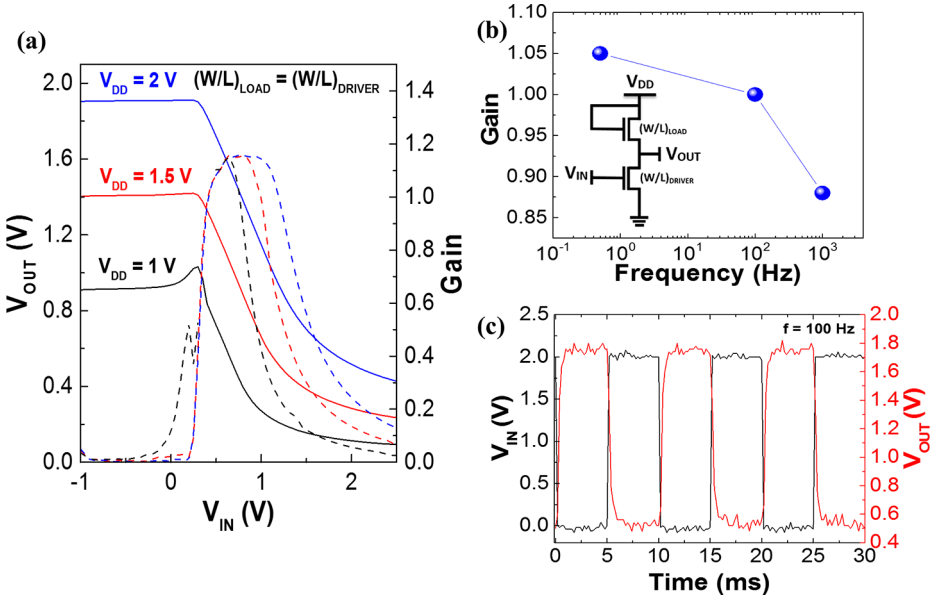


**Figure 7.** (a) Voltage transfer characteristics and signal gain of the diode-connected inverter with $(HfO_x|HfO_x)$/IGZO TFTs. (b) Voltage gain for different frequencies and (c) a dynamic switching behavior of the inverter under AC square waves at 100 Hz.



DOI: 10.1021/acsami.7b11752
ACS Appl. Mater. Interfaces XXXX, XXX, XXX−XXX

**3.5. Diode-Connected Inverter.** Because the ($HfO_x$|$HfO_x$)/IGZO thin film transistors revealed the best electrical performance, a good stability and uniformity, we applied them in a basic building block, an inverter. The structure of this circuit was performed using two TFTs, the load and the driver, with the same $W/L$ = 11. The load TFT had the gate short-circuited with the drain in order to work as a resistor. The voltage transfer characteristics (VTC) of the obtained inverter were measured at various supplied voltages ($V_{DD}$), 1, 1.5, and 2 V, as shown in Figure 7a. It is noticed that the output high voltage, 1.9 V, is close to the $V_{DD}$, 2 V, and the output low voltage is 0.3 V, when was supposed to be 0 V. For this configuration the high output value is $V_{DD} - V_{T\ (LOAD)}$ and for the low output value a higher than 0 V is expected, as the load TFT cannot be completely turned OFF. The inverter exhibits a maximum gain ($-\partial V_{OUT}/\partial V_{IN}$) of 1.15 for the different supplied voltages, but due to the use of two identical TFTs the expected value was 1. This difference can be explained by a slight mismatch between the two TFTs, as depicted in Figure S11.

To investigate the alternative current (AC) characteristic of the inverter, we measured the dynamic behavior under AC square wave for different frequencies and the result is shown in Figure 7b. The device exhibited good inversion properties, however, the gain decreased slightly with the increase of the frequency, more precisely to 1 kHz. The gain values are smaller in the dynamic measurements when compared with the values in the static VTC curve because a buffer was not used to provide enough current for full voltage swing, losing some current in the cables. To improve the AC results, some tests of etching should be done to produce structures suitable for these measurements. Figure 7c shows that the device can achieve sufficient switching speeds for wearable applications.

## 4. CONCLUSIONS

In this work, we have demonstrated for the first time the combustion solution synthesis alliance with UV treatment in $HfO_x$ dielectric thin films and multilayer thin films using $AlO_x$ and $HfO_x$ at low temperatures (150 °C) and their implementation in electronic structures. The physical properties of the single layers and multilayers were investigated using a wide range of characterization techniques that revealed smooth surface (<1.2 nm), high-$\kappa$ (13.5), high transparency (>89%), low leakage currents, and high breakdown voltages (>2.7 MV $cm^{-1}$). The multilayer MIS devices exhibit an improvement by presenting low capacitance dependence at low frequencies when compared with the single layers. In terms of thin film transistors (TFTs), the ($HfO_x$|$HfO_x$)/IGZO TFTs showed the best electrical performance with low voltage operation, low subthreshold slope (0.066 ± 0.01 V $dec^{-1}$), 0 V turn-on voltage, a high saturation mobility (43.9 ± 1.1 $cm^2\ V^{-1}\ s^{-1}$) and current ratio of 1 × $10^6$. This device also presented good stability over time (2 months) and under positive gate bias stress (PBS) for 1 h, having a maximum threshold voltage variation of 0.06 V. These devices were applied in a diode-connected inverter showing good switching speed at 100 Hz with a maximum gain of 1 at 2 V. Taking in consideration the excellent results achieved in this report, the next step will be the implementation in large-area processing techniques.

## ■ ASSOCIATED CONTENT

### Supporting Information

The Supporting Information is available free of charge on the ACS Publications website at DOI: 10.1021/acsami.7b11752.

Relevant data related to the production of high-$\kappa$ dielectric thin films from solution combustion synthesis combined with ultraviolet (UV) treatment and their application in TFTs; Figure S1 and S2 show XRD diffractograms and the FTIR spectra of multilayer dielectric thin films, respectively. Figure S3 depicts AFM surface morphology of multilayer dielectric thin films; Figure S4 show the SEM-FIB cross-section image of multilayer dielectric thin films to determine film thickness; Figure S5 depicts the influence of the fuel in $AlO_x$ thin film thickness for different concentrations assisted by UV treatment; Figure S6 show the capacitance−frequency, capacitance−voltage, and current density ($J$) characteristics of Al/p-type Si/(Dielectric)/Al MIS capacitors with single and multilayer dielectric thin films; Table S1 show the summary of dielectric properties obtained for the capacitors; Figure S7 depicts the typical output curves of all dielectrics conditions applied in TFTs; Figure S8 and Table S2 show the electrical characteristics obtained for the different dielectric conditions applied in IGZO TFTs after 2 months in air environment; Figures S9 and S10 show the transfer curves after stress and recovery measurements of the dielectric bilayers applied in IGZO TFTs; Figure S11 depicted the transfer curves of TFTs used in the diode-connected inverter (PDF)

## ■ AUTHOR INFORMATION


### Corresponding Authors

*E-mail: elvira.fortunato@fct.unl.pt.

*E-mail: ritasba@fct.unl.pt.

### ORCID

Rita Branquinho: 0000-0001-9771-8366

Elvira Fortunato: 0000-0002-4202-7047


### Notes

The authors declare no competing financial interest.

## ■ ACKNOWLEDGMENTS

This work is funded by FEDER funds through the COMPETE 2020 Programme and National Funds through FCT - Portuguese Foundation for Science and Technology under project number POCI-01-0145-FEDER-007688, Reference UID/CTM/50025. European Community H2020 NMP-22-2015 project 1D-NEON Grant Agreement 685758. A.K. acknowledges FCT-MEC for a postdoctoral grant (Grant SFRH/BPD/99136/2013). J.M. acknowledges FCT-MEC for a doctoral grant (Grant SFRH/BD/122286/2016). E.C. acknowledges FCT-MEC for a doctoral grant (Grant SFRH/BD/116047/2016) and IDS-FunMat-INNO project FPA2016/EIT/EIT RawMaterials Grant Agreement 15015. The authors acknowledge J. V. Pinto and S. Pereira for XRD, D. Nunes for SEM-FIB, and T. Sequeira for AFM measurements.

## ■ REFERENCES

(1) Lorenz, M.; Ramachandra Rao, M. S.; Venkatesan, T.; Fortunato, E.; Barquinha, P.; Branquinho, R.; Salgueiro, D.; Martins, R.; Carlos, E.; Liu, A.; Shan, F. K.; Grundmann, M.; Boschker, H.; Mukherjee, J.;



DOI: 10.1021/acsami.7b11752
ACS Appl. Mater. Interfaces XXXX, XXX, XXX−XXX

Priyadarshini, M.; DasGupta, N.; Rogers, D. J.; Teherani, F. H.; Sandana, E. V.; Bove, P.; Rietwyk, K.; Zaban, A.; Veziridis, A.; Weidenkaff, A.; Muralidhar, M.; Murakami, M.; Abel, S.; Fompeyrine, J.; Zuniga-Perez, J.; Ramesh, R.; Spaldin, N. A.; Ostanin, S.; Borisov, V.; Mertig, I.; Lazenka, V.; Srinivasan, G.; Prellier, W.; Uchida, M.; Kawasaki, M.; Pentcheva, R.; Gegenwart, P.; Miletto Granozio, F.; Fontcuberta, J.; Pryds, N. The 2016 Oxide Electronic Materials and Oxide Interfaces Roadmap. *J. Phys. D: Appl. Phys.* **2016**, *49* (43), 433001.

(2) Fortunato, E.; Barquinha, P.; Martins, R. Oxide Semiconductor Thin-Film Transistors: A Review of Recent Advances. *Adv. Mater.* **2012**, *24* (22), 2945−2986.

(3) Park, S.; Kim, C.-H.; Lee, W.-J.; Sung, S.; Yoon, M.-H. Sol-Gel Metal Oxide Dielectrics for All-Solution-Processed Electronics. *Mater. Sci. Eng., R* **2017**, *114*, 1−22.

(4) Glynn, C.; O'Dwyer, C. Solution Processable Metal Oxide Thin Film Deposition and Material Growth for Electronic and Photonic Devices. *Adv. Mater. Interfaces* **2017**, *4* (2), 1600610.

(5) Nayak, P. K.; Busani, T.; Elamurugu, E.; Barquinha, P.; Martins, R.; Hong, Y.; Fortunato, E. Zinc Concentration Dependence Study of Solution Processed Amorphous Indium Gallium Zinc Oxide Thin Film Transistors Using High-K Dielectric. *Appl. Phys. Lett.* **2010**, *97* (18), 183504.

(6) Salgueiro, D.; Kiazadeh, A.; Branquinho, R.; Santos, L.; Barquinha, P.; Martins, R.; Fortunato, E. Solution Based Zinc Tin Oxide TFTs: The Dual Role of the Organic Solvent. *J. Phys. D: Appl. Phys.* **2017**, *50* (6), 65106.

(7) Lee, W.-J.; Park, W.-T.; Park, S.; Sung, S.; Noh, Y.-Y.; Yoon, M.-H. Large-Scale Precise Printing of Ultrathin Sol-Gel Oxide Dielectrics for Directly Patterned Solution-Processed Metal Oxide Transistor Arrays. *Adv. Mater.* **2015**, *27* (34), 5043−5048.

(8) Kim, Y.-H.; Heo, J.-S.; Kim, T.-H.; Park, S.; Yoon, M.-H.; Kim, J.; Oh, M. S.; Yi, G.-R.; Noh, Y.-Y.; Park, S. K. Flexible Metal-Oxide Devices Made by Room-Temperature Photochemical Activation of Sol−gel Films. *Nature* **2012**, *489* (7414), 128−132.

(9) Kim, M.-G.; Kanatzidis, M. G.; Facchetti, A.; Marks, T. J. Low-Temperature Fabrication of High-Performance Metal Oxide Thin-Film Electronics via Combustion Processing. *Nat. Mater.* **2011**, *10* (5), 382−388.

(10) Park, S.; Kim, K. H.; Jo, J. W.; Sung, S.; Kim, K. T.; Lee, W. J.; Kim, J.; Kim, H. J.; Yi, G. R.; Kim, Y. H.; Yoon, M. H.; Park, S. K. In-Depth Studies on Rapid Photochemical Activation of Various Sol-Gel Metal Oxide Films for Flexible Transparent Electronics. *Adv. Funct. Mater.* **2015**, *25* (19), 2807−2815.

(11) Carlos, E.; Branquinho, R.; Kiazadeh, A.; Barquinha, P.; Martins, R.; Fortunato, E. UV-Mediated Photochemical Treatment for Low-Temperature Oxide-Based Thin-Film Transistors. *ACS Appl. Mater. Interfaces* **2016**, *8* (45), 31100−31108.

(12) Dey, A.; Kalita, A.; Iyer, P. K. High-Performance N - Channel Organic Thin-Film Transistor Based on Naphthalene Diimide. *ACS Appl. Mater. Interfaces* **2014**, *6*, 12295−12301.

(13) Kim, S. J.; Jang, M.; Yang, H. Y.; Cho, J.; Lim, H. S.; Yang, H.; Lim, J. A. Instantaneous Pulsed-Light Cross-Linking of a Polymer Gate Dielectric for Flexible Organic Thin-Film Transistors. *ACS Appl. Mater. Interfaces* **2017**, *9* (13), 11721−11731.

(14) Li, Y.; Lan, L.; Xiao, P.; Sun, S.; Lin, Z.; Song, W.; Song, E.; Gao, P.; Wu, W.; Peng, J. Coffee-Ring Defined Short Channels for Inkjet-Printed Metal Oxide Thin-Film Transistors. *ACS Appl. Mater. Interfaces* **2016**, *8* (30), 19643−19648.

(15) Liu, A.; Guo, Z.; Liu, G.; Zhu, C.; Zhu, H.; Shin, B.; Fortunato, E.; Martins, R.; Shan, F. Redox Chloride Elimination Reaction: Facile Solution Route for Indium-Free, Low-Voltage, and High-Performance Transistors. *Adv. Electron. Mater.* **2017**, *3*, 1600513.

(16) Zhang, F.; Liu, G.; Liu, A.; Shin, B.; Shan, F. Solution-Processed Hafnium Oxide Dielectric Thin Films for Thin-Film Transistors Applications. *Ceram. Int.* **2015**, *41* (10), 13218−13223.

(17) Kim, Y. G.; Avis, C.; Jang, J. Low Voltage Driven, Stable Solution-Processed Zinc-Tin-Oxide TFT with HfOy and AlOx Stack Gate Dielectric. *ECS Solid State Lett.* **2012**, *1* (2), Q23−Q25.

(18) Park, J. H.; Lee, S. J.; Lee, T. I.; Kim, J. H.; Kim, C.-H.; Chae, G. S.; Ham, M.-H.; Baik, H. K.; Myoung, J.-M. All-Solution-Processed, Transparent Thin-Film Transistors Based on Metal Oxides and Single-Walled Carbon Nanotubes. *J. Mater. Chem. C* **2013**, *1* (9), 1840−1845.

(19) Branquinho, R.; Salgueiro, D.; Santos, L.; Barquinha, P.; Pereira, L.; Martins, R.; Fortunato, E. Aqueous Combustion Synthesis of Aluminum Oxide Thin Films and Application as Gate Dielectric in GZTO Solution-Based TFTs. *ACS Appl. Mater. Interfaces* **2014**, *6* (22), 19592−19599.

(20) Han, S. W.; Park, J. H.; Yoo, Y. B.; Lee, K. H.; Kim, K. H.; Baik, H. K. Solution-Processed Laminated ZrO2/Al2O3 Dielectric for Low-Voltage Indium Zinc Oxide Thin-Film Transistors. *J. Sol-Gel Sci. Technol.* **2017**, *81* (2), 570−575.

(21) Liu, A.; Liu, G. X.; Zhu, H. H.; Xu, F.; Fortunato, E.; Martins, R.; Shan, F. K. Fully Solution-Processed Low-Voltage Aqueous In2O3 Thin-Film Transistors Using an Ultrathin ZrOx Dielectric. *ACS Appl. Mater. Interfaces* **2014**, *6* (20), 17364−17369.

(22) Pereira, L.; Barquinha, P.; Fortunato, E.; Martins, R. Influence of the Oxygen/argon Ratio on the Properties of Sputtered Hafnium Oxide. *Mater. Sci. Eng., B* **2005**, *118* (1−3), 210−213.

(23) Wang, H.; Sun, T.; Xu, W.; Xie, F.; Ye, L.; Xiao, Y.; Wang, Y.; Chen, J.; Xu, J. Low-Temperature Facile Solution-Processed Gate Dielectric for Combustion Derived Oxide Thin Film Transistors. *RSC Adv.* **2014**, *4* (97), 54729−54739.

(24) Park, S.; Kim, K.-H.; Jo, J.-W.; Sung, S.; Kim, K.-T.; Lee, W.-J.; Kim, J.; Kim, H. J.; Yi, G.-R.; Kim, Y.-H.; Yoon, M.-H.; Park, S. K. In-Depth Studies on Rapid Photochemical Activation of Various Sol-Gel Metal Oxide Films for Flexible Transparent Electronics. *Adv. Funct. Mater.* **2015**, *25* (19), 2807−2815.

(25) Avis, C.; Kim, Y. G.; Jang, J. Solution Processed Hafnium Oxide as a Gate Insulator for Low-Voltage Oxide Thin-Film Transistors. *J. Mater. Chem.* **2012**, *22* (34), 17415.

(26) Gao, Y. N.; Xu, Y. L.; Lu, J. G.; Zhang, J. H.; Li, X. F. Solution Processable Amorphous Hafnium Silicate Dielectrics and Their Application in Oxide Thin Film Transistors. *J. Mater. Chem. C* **2015**, *3* (43), 11497−11504.

(27) Esro, M.; Vourlias, G.; Somerton, C.; Milne, W. I.; Adamopoulos, G. High-Mobility ZnO Thin Film Transistors Based on Solution-Processed Hafnium Oxide Gate Dielectrics. *Adv. Funct. Mater.* **2015**, *25* (1), 134−141.

(28) Kiazadeh, A.; Gomes, H. L.; Barquinha, P.; Martins, J.; Rovisco, A.; Pinto, J. V.; Martins, R.; Fortunato, E. Improving Positive and Negative Bias Illumination Stress Stability in Parylene Passivated IGZO Transistors. *Appl. Phys. Lett.* **2016**, *109* (5), 051606.

(29) Weng, J.; Chen, W.; Xia, W.; Zhang, J.; Jiang, Y.; Zhu, G. Low-Temperature Solution-Based Fabrication of High-K HfO2 Dielectric Thin Films via Combustion Process. *J. Sol-Gel Sci. Technol.* **2017**, *81*, 662−668.

(30) González-Cortés, S. L.; Imbert, F. E. Fundamentals, Properties and Applications of Solid Catalysts Prepared by Solution Combustion Synthesis (SCS). *Appl. Catal., A* **2013**, *452*, 117−131.

(31) González-Cortés, S. L.; Imbert, F. E. Advanced Synthesis of Materials for Intermediate-Temperature Solid Oxide Fuel Cells. *Appl. Catal., A* **2013**, *452* (4), 117−131.

(32) González-Cortés, S. L.; Imbert, F. E. Fundamentals, Properties and Applications of Solid Catalysts Prepared by Solution Combustion Synthesis (SCS). *Appl. Catal., A* **2013**, *452*, 117−131.

(33) Jain, S. R.; Adiga, K. C.; Pai Verneker, V. R. A New Approach to Thermochemical Calculations of Condensed Fuel-Oxidizer Mixtures. *Combust. Flame* **1981**, *40*, 71−79.

(34) Branquinho, R.; Salgueiro, D.; Santa, A.; Kiazadeh, A.; Barquinha, P.; Pereira, L.; Martins, R.; Fortunato, E. Towards Environmental Friendly Solution-Based ZTO/AlO X TFTs. *Semicond. Sci. Technol.* **2015**, *30* (2), 024007.

(35) Epifani, M.; Melissano, E.; Pace, G.; Schioppa, M. Precursors for the Combustion Synthesis of Metal Oxides from the Sol−gel Processing of Metal Complexes. *J. Eur. Ceram. Soc.* **2007**, *27* (1), 115−123.



DOI: 10.1021/acsami.7b11752
ACS Appl. Mater. Interfaces XXXX, XXX, XXX−XXX

786 (36) Faber, H.; Lin, Y.; Thomas, S. R.; Zhao, K.; Pliatsikas, N.;
787 McLachlan, M. A.; Amassian, A.; Patsalas, P. A.; Anthopoulos, T. D.
788 Indium Oxide Thin-Film Transistors Processed at Low Temperature
789 via Ultrasonic Spray Pyrolysis. *ACS Appl. Mater. Interfaces* **2015**, *7* (1),
790 782−790.
791 (37) Neumayer, D. A.; Cartier, E. Materials Characterization of
792 ZrO2−SiO2 and HfO2−SiO2 Binary Oxides Deposited by Chemical
793 Solution Deposition. *J. Appl. Phys.* **2001**, *90* (4), 1801−1808.
794 (38) Toledano-Luque, M.; San Andrés, E.; Olea, J.; del Prado, A.;
795 Mártil, I.; Bohne, W.; Röhrich, J.; Strub, E. Hafnium Oxide Thin Films
796 Deposited by High Pressure Reactive Sputtering in Atmosphere
797 Formed with Different Ar/O2 Ratios. *Mater. Sci. Semicond. Process.*
798 **2006**, *9* (6), 1020−1024.
799 (39) Reyes, J. M.; Perez Ramos, B. M.; Islas, C. Z.; Arriaga, W. C.;
800 Quintero, P. R.; Jacome, a. T. Chemical and Morphological
801 Characteristics of ALD Al2O3 Thin-Film Surfaces after Immersion
802 in pH Buffer Solutions. *J. Electrochem. Soc.* **2013**, *160* (10), B201−
803 B206.
804 (40) Chang, Y.-H.; Yu, M.-J.; Lin, R.-P.; Hsu, C.-P.; Hou, T.-H.
805 Abnormal Positive Bias Stress Instability of In−Ga−Zn−O Thin-Film
806 Transistors with Low-Temperature Al2O3 Gate Dielectric. *Appl. Phys.*
807 *Lett.* **2016**, *108* (3), 033502.



DOI: 10.1021/acsami.7b11752
*ACS Appl. Mater. Interfaces* XXXX, XXX, XXX−XXX